

A Three-Dimensional Calculation of Atmospheric Neutrino Fluxes¹

Yaroslav Tserkovnyak²

Physics Department, Harvard University, Cambridge MA 02138

Robert Komar, Christian Nally, Chris Waltham³

*Department of Physics and Astronomy, University of British Columbia, Vancouver
B.C., Canada V6T 1Z1*

Abstract

We present a three-dimensional calculation of atmospheric neutrino fluxes using accurate models of the geomagnetic field, hadronic interactions, tracking and decays. Results are presented for the Super-Kamiokande (SK) and Sudbury Neutrino Observatory (SNO) sites using the GEANT-FLUKA hadronic code. We make a comparison with previous one-dimensional calculations and other three-dimensional results. The recently reported geometrical enhancement of low energy, horizontal neutrinos is confirmed. The effect on observed leptons is however, restricted to a small overall increase in flux. We report east-west asymmetries for each of the neutrino species.

Revised draft for submission to Astroparticle Physics

PACS Numbers: 96.40Tv,98.70.S,96.40Kk,14.60.P

¹ The work was supported by the Natural Science and Engineering Research Council of Canada (NSERC).

² Supported in part by a Faculty of Science scholarship from the University of British Columbia and a summer studentship from the TRIUMF laboratory, Vancouver

³ Corresponding author; email: waltham@physics.ubc.ca

1 Introduction

Atmospheric neutrinos are produced constantly by the interaction of primary cosmic rays with nuclei of the earth's upper atmosphere. These primary interactions produce pions and kaons which decay into neutrinos and muons; the muons themselves may decay into additional detectable neutrinos if they don't have enough energy to reach the ground. The following reaction sequence is typical:

$$p + {}^{14}\text{N} \rightarrow \pi^+(K^+) + X; \quad \pi^+(K^+) \rightarrow \mu^+\nu_\mu; \quad \mu^+ \rightarrow e^+\bar{\nu}_\mu\nu_e \quad (1)$$

The primary cosmic rays are mostly protons, with a small fraction of heavier nuclei. The energy spectrum has the approximate form $E^{-2.7}$ over the energy range applicable to the production of detectable neutrinos. The spectrum is modified at low energies by solar activity, which varies slowly with time. At large distances from the earth the primary flux is isotropic. Closer to the earth the flux is reduced at low energies in an angle-dependent way by the geomagnetic field.

Atmospheric neutrino fluxes are such that the rate of detection is of the order 100 per kiloton of detector per year. They were the first naturally occurring neutrinos to be observed, some thirty years ago[1]. Since then they have generated interest, first as a critical background in nucleon-decay searches, and more recently in their own right as the means by which neutrino oscillations were discovered[2].

The most obvious predictions of the reaction sequence above is that (a) there will be two muon neutrinos for each electron neutrino, (b) the antineutrino to neutrino ratio will be about unity for muons and 1.3 ($\approx \pi^+/\pi^-$ ratio) for electrons. In addition to the numerology, we can also make a broad statement about neutrino isotropy. At high energies the primary cosmic ray flux becomes isotropic in angle, as geomagnetic effects become small. It is therefore expected that the angular distribution of atmospheric neutrinos will tend at high energy to isotropy, except for a horizontal enhancement due to the increased meson decay path in the atmosphere.

Prediction (a) has not been borne out by recent experiments which measure a muon to electron ratio which is both a factor two too small and which is strongly zenith angle (and therefore pathlength) dependent[2]. This is evidence for neutrino oscillations and a non-zero neutrino mass. Prediction (b) has not yet been tested; there has been no measurement of the antineutrino to neutrino ratios. Given the tremendous implications of this neutrino mass signal, it is plainly important to model atmospheric neutrinos as well as possible, and examine very closely any mundane effect which may affect the result.

There have already been several successful calculations of atmospheric neutrino fluxes. Most have been one-dimensional “slab” models with geomagnetic cut-offs, chosen for calculational simplicity. This approximation is based on well-founded principles and not thought to introduce serious error, except in the angular distributions at the lowest detectable energies. We chose to pursue a three-dimensional calculation, this route now being feasible because available computing power has increased dramatically since the first atmospheric neutrino codes were started.

There are three major independent 1-D calculations of atmospheric neutrino fluxes which predate this work. Two of them were being updated until very recently; that of the Bartol group (“BGS” [3]) and that of the (Super-)Kamiokande group (“HKHM” [4]). Bugaev and Naumov (“BN”) is an older work [5]. Lee and Koh [6] (“LK”) was an early attempt to make the BGS code three-dimensional; it had some problems and was not pursued [7]. The main justification for the 1-D approximation is that the transverse momentum from pion or muon decay is reckoned to be small enough (10s of MeV/c) to obviate the need to consider more dimensions when the threshold of the atmospheric neutrino detectors is at least 100 MeV/c.

As our work was being done, Battistoni *et al.*[8] published the first results from a 3-D calculation. They reported a geometrical enhancement of low energy, horizontal neutrinos, not seen in 1-D calculations. The origins of this effect were subsequently explained in a pedagogical paper by Lipari [9]. At the time we did not see this effect because we had expanded our detector size for calculational efficiency and had unwittingly washed out the enhancement. Reducing the vertical extent of the detector revealed the effect to be there. The impact on the observed leptons is however, restricted to a small overall increase in flux and a small but significant improvement in understanding the so-called “east-west effect” seen in the Super-Kamiokande (SK) data[10,11]. Other than this, neither our work nor Battistoni’s report a large difference between the 1-D and 3-D approaches.

In this work we compare our calculations with those of Bartol 1-D model[3] for the SK site, those of the 3-D model of Battistoni[8] for SK and northern sites, and with newer 3-D work of Wentz[13] and the HKKM[14] group.

In section 2 the details of the calculation are described. We outline the input parameters for the primary flux, the geomagnetic field, and the atmosphere. We discuss tracking issues and dealing with secondary particles. The question of hadronic interactions is considered in some detail, with comparisons made between various codes. Lastly we outline the findings of other 3-D work on angular distributions.

In section 3 we present our results for the SK and Sudbury Neutrino Observatory (SNO)[15] sites and compare them with other calculations. The magnetic latitude for SK is 27° N[14], and that for SNO is 57° N.

2 Theory

2.1 Introduction

In the absence of magnetic fields and at high energy, the production of neutrinos by cosmic ray interactions in the earth’s atmosphere can be calculated to a fair approximation by semi-analytic models[7,16]. This is especially true at high energies, where the primary proton (or heavier nucleus), intermediate meson, and decay product muons and neutrinos, are all essentially co-linear. The mesons - mostly pions and kaons - have a choice of interaction or decay in the atmosphere, and the muons - if of low enough energy - can also decay. The cosmic ray primaries are isotropic; the only deviation from isotropy in the neutrinos is a horizontal enhancement due to a large slant range in the atmosphere, allowing more to decay.

$$P_{\nu_{\mu}+\bar{\nu}_{\mu}}^{\pi,K,\mu} \sim E^{-\gamma} \cdot \left(\frac{1}{1 + \frac{6E \cos \theta}{121\text{GeV}}} + \frac{0.213}{1 + \frac{1.44E \cos \theta}{897\text{GeV}}} \right) (\text{m}^{-2} \cdot \text{sr}^{-1} \cdot \text{s}^{-1} \cdot \text{GeV}^{-1})$$

This expression, due to Volkova[16], gives the muon neutrino and antineutrino flux $P_{\nu_{\mu}+\bar{\nu}_{\mu}}^{\pi,K,\mu}$ which results from π , K and μ decay. It is good to a few % at energies above 100 GeV and angles not close to horizontal ($|\cos \theta| > 0.2$) where the curvature of the earth becomes important. We do not use this formula in our calculation, but it encapsulates the basic features of the neutrino flux. At lower energies the neutrino spectrum follows that of the primaries, $E^{-\gamma}$, where $\gamma \approx 2.7$, and is isotropic. At higher energies the neutrino spectrum goes as $E^{-(\gamma+1)}/\cos \theta$ due to competition between interaction and decay in the atmosphere. The first term in the parenthesis accounts for pion decay, the second, kaon decay. At low energies one has to account for the geomagnetic field, muon decay, and non-colinear decay products.

2.2 The Basics of Atmospheric Neutrino Flux Calculations

There are two basic approaches to these calculations; they are either one-dimensional (“slab”) models or three-dimensional models like the one pre-

sented here. The calculations can be split into different parts, some of which are common between the two approaches.

- 3-D: Start at the top of the atmosphere close to the location of a detector and take primaries with energies according to the interstellar spectrum but only above the local cutoff (which depends on the direction of the primary). 1-D calculations only need primaries in direct line of sight to the detector. Check if earth shadowing prevents this trajectory by reversing charge of primary and tracking backwards. If this track intersects the earth's surface this primary is rejected.
- Allow the primaries to interact with a model of the atmosphere, using one or more packages of hadronic interaction codes, producing charged secondaries and neutrinos.
- Track the charged secondaries in the earth's magnetic field (3-D). In the 1-D model the secondaries are tracked along the primary direction.
- Allow secondaries to decay into neutrinos.
- Check if the neutrino has crossed the designated detector area (inflated in such a way as to improve statistics without washing out local effects).
- Bin neutrinos and calculate fluxes as a function of neutrino type, energy, direction and solar activity.
- Calculate interaction rates and angular distributions of leptons observed in the detectors.

The statistical accuracy and number of bins is typically limited by computation time in the 3-D case.

2.3 Primary Flux

For the primary cosmic ray flux we use the same parameterization as the Bartol calculation [19], and assume medium solar activity. This form has been superseded by a new fit by the Bartol group (Gaisser *et al.*[20]) which predicts a 10% increase in the primaries which produce sub-GeV neutrinos.

2.4 Geomagnetic Field

The geomagnetic field is calculated using a 10th order multipole expansion, with spherical harmonic coefficients taken from the IGRF 1995 model [21]. Errors in the field at the earth's surface are less than 25 nT (<0.1%). A detailed discussion of geomagnetic effects appears in a paper by Gaisser *et al.* [7].

For any given position on the earth's surface, an angular map may be made

showing the minimum rigidity required for a positively charged particle, starting from a large distance away, to reach the surface from that angle. The resulting cutoff maps for SNO and SK are shown in Fig.1; in terms of cardinal points the x-axis is ordered N-W-S-E-N. The plot for the SK site is identical to that obtained by Honda et al. [4]. There is much less structure in the more northerly SNO site, with the cutoffs from the north being much lower than those from the south (the opposite of the SK case), and very little of the east-west asymmetry seen at SK[10]. The maps can be understood in terms of the angle of the geomagnetic field as seen from the detector position: the positions of the SNO and SK sites are shown in Fig.2. Because the dip angle at the SK site is small, there is a strong deficit of primaries coming from the east. At the SNO site, the dip angle is large, so the east-west asymmetry is small, and there is almost no reduction in primaries coming from above. However, where the line-of-sight intersects the geomagnetic field at 90° , there is an increase in the cutoff. This occurs for near-horizontal primaries, and for those coming from a tilted ring around middle latitudes in the southern hemisphere.

Figure 3 shows how the geomagnetic field affects the spectrum of cosmic ray primaries reaching the upper atmosphere. Maps of the intensities of cosmic ray primaries on the earth's surface (averaged over all incident angles and shown as a fraction of the zero geomagnetic field case) are shown for various momenta. The effect of the geomagnetic field is of course strongest at low energies and fades away by about 20 GeV at the SNO site, and 40 GeV at the SK site. Note how the SNO site sits on the edge of a region where the low energy primary flux is changing very rapidly with latitude. This provides a challenge for the 3-D modeller as the detector cannot be arbitrarily enlarged to improve statistics.

2.5 Tracking Primaries and Secondaries

Far away from the earth, where the geomagnetic field merges into the interplanetary field, the flux of cosmic rays is essentially isotropic[17]. As a cosmic ray approaches the earth, it is progressively bent by the geomagnetic field and, if it is of low enough rigidity (momentum/charge) it will be turned away. A typical value is that required for a particle to orbit the earth, just above the surface, at its magnetic equator, with a locally horizontal field of mean strength $30 \mu\text{T}$; this rigidity is $60 \text{ GV}/c$ (i.e. an energy of 60 GeV for a proton). In addition, some parts of the earth's surface are, for certain angles and rigidities, in shadow from other parts of the earth.

We model these effects in a manner similar to that of the HKHM group [4]. The primary flux at large distances from the earth only depends on energy (and time - due to a small solar modulation, which we ignore for now) and can

be written as $\phi_p^\infty(E)$. The primary flux which strikes the earth’s atmosphere, however, depends on position and angle: $\phi_p(E, \mathbf{x}, \Omega)$. Invoking Liouville’s theorem, which is applicable as long as the magnetic field can be considered static, yields the simple form:

$$\phi_p(E, \mathbf{x}, \Omega) = \phi_p^\infty(E) \text{ for allowed paths} \quad (2)$$

$$= 0 \text{ for forbidden paths} \quad (3)$$

To decide which paths are allowed or forbidden, a check is made for reflection in the geomagnetic field and shadowing by the earth before a positively charged primary is tracked through the atmosphere. An equivalent negatively charged particle is tracked backwards to see if its trajectory reaches a very large distance from the earth ($10 R_E$, where R_E is the earth’s radius) without intersecting with it. If it did, such a trajectory is allowed; if not, it is rejected.

The atmospheric density is calculated according to Linsley’s compilation of data[22]. Inside the atmosphere both primaries and secondaries were tracked in steps of 1 km (Fig. 4). In each case helical steps were taken, using the magnetic field at the centre of the helix and assuming it to be uniform over the step. In order to keep statistics sensible, detector areas were artificially increased to a rectangle 10° by 40° with the shorter side pointing to magnetic north to reduce the washing out of local geomagnetic effects. The “detector” was considered to be a flat sheet as any increase in the thickness was found to mask the geometrical horizontal enhancement discovered by Battistoni *et al.*[8].

2.6 Hadronic Interactions

In order to calculate hadronic interactions, we start with experimental parameterization for hadron-hadron cross-sections (from the CORSIKA[23] air shower package). Hadron-nucleus and nucleus-nucleus cross-sections were calculated using Glauber theory (instead of $A^{2/3}$ re-scaling as used in GEANT).

Secondaries were generated using several standard hadronic packages. We used generators CALOR, GEANT-FLUKA and GHEISHA within GEANT 3.21[24,25], and stand-alone generator FRITIOF and decay routine JETSET[26]. In order to compare the results from these packages, we calculate several functions of the pion production cross sections in the energy range relevant to sub-GeV neutrinos. In this we followed the published comparisons of Gaisser *et al.* [7]. The crucial discriminants are the spectrum-weighted moments, the

“Z”-factors:

$$Z_{p \rightarrow \pi^\pm} = \int_0^1 dx \cdot x^{1.7} \frac{dn_{\pi^\pm}(x, E_N)}{dx} \quad (4)$$

where $x = E_\pi/E_N$, and E_N is the total energy of the incident nucleon in the lab system and E_π is the energy of the secondary pion. The values of these factors determine how many charged pions are produced at a given energy, and it is these pions which decay into neutrinos. In Fig.5 we plot these moments for charged pions for three hadronic packages. The GEANT-FLUKA[25] package gives the highest value, and GHEISHA [24] the lowest. In the middle lie CALOR[24] and FRITIOF[26], although FRITIOF gives the highest multiplicities. It is a combination of these (CALOR below 10 GeV/c and FRITIOF above), which most closely reproduces the spectrum-weighted moments in the TARGET code of BGS[7]. CALOR and GEANT-FLUKA are not independent; the two codes are identical above 10 GeV. CALOR uses GEANT-FLUKA pion and nucleon routines phased in from 2 to 10 GeV. Kaon and antinucleon routines in the two codes are identical. In terms of neutrino production the three hadronic packages produced results with very similar distributions but with different overall rates. GEANT-FLUKA and CALOR/FRITIOF give similar overall rates while GHEISHA leads to a much smaller neutrino flux (about 40% of the rate calculated with GEANT-FLUKA).

The quantity which indicates best the neutrino yield is the spectrum-weighted production of charged pions $Y(\pi^\pm)E_0^{-1.7}$, where Y is the multiplicity per interaction and E_0 the primary energy. In Fig.6 we compare the spectrum-weighted pion production per nucleon for CALOR/FRITIOF and for TARGET. The pion momentum range of 3-4 GeV/c is chosen as these are the pions which produce neutrinos with energies around 1 GeV[7]. The value of this parameter integrated on a logarithmic scale in the primary energy is roughly proportional to the measurable neutrino flux. Due in part to different pion multiplicities, our CALOR/FRITIOF combination gives an integral which is 21% lower than TARGET. Hence we expect that differences in hadronic codes, everything else being equal, will give us a neutrino flux at 1 GeV which is about 21% lower than that of BGS when we use CALOR/FRITIOF hadronic code. Furthermore, GEANT-FLUKA produces somewhat smaller unweighted charged pion multiplicities than FRITIOF, with consequently smaller neutrino fluxes. See Section 3.1 below.

2.7 East-West Effect

A major systematic effect on atmospheric neutrino data is the geomagnetic field. This is particularly true at more southerly sites like SK, where the most

pronounced feature is an east-west asymmetry. To understand this asymmetry lends significant confidence in the interpretation of the data. As Lipari has pointed out[11], there is a hierarchy in the asymmetries of the different neutrino species, due to the difference in the bending of primaries and secondaries (Fig. 7). The ν_e arises from the decay of positively charged secondaries and so the asymmetry is the largest. The $\bar{\nu}_e$ arises from the decay of negatively charged secondaries and so the asymmetry is the smallest. In between lie the $\bar{\nu}_\mu$ and ν_μ , with the former having a larger asymmetry as some of them arise from decaying positive muons which are more deflected than neutrinos produced directly from pion decays.

The effect is not easy to find in the data without energy and directional cuts. Lipari proposes a using neutrinos which produce leptons with energies of 0.4-3 GeV with zenith angles $|\cos\theta_l| < 0.5$. The standard definition of the asymmetry A in terms of the numbers of neutrinos $N_{E,W}$ is as follows.

$$A = \frac{N_E - N_W}{N_E + N_W} \quad (5)$$

With a 3-D calculation he obtains an electron E-W asymmetry of 0.224 and a muon asymmetry of 0.091. The corresponding experimental values[10] are in good agreement, being 0.21 ± 0.04 and 0.08 ± 0.04 respectively.

2.8 Horizontal Enhancement

The first three-dimensional calculations revealed a geometrical effect not anticipated in one-dimensional models. For low energy primaries ($\ll 1$ GeV) the secondary particles have almost no directional correlation with their parents (Fig. 8). For a detector far from the earth's centre, this produces a strong enhancement for particles detected coming from near the horizontal [8,9]. Unfortunately this effect is very hard to observe for three reasons: (a) the flux of low energy secondary neutrinos is small, (b) the cross sections for interaction in a detector is small, and (c) the correlation between the directions of the neutrino and the detected lepton is weak.

3 Results

Our results using the GEANT-FLUKA hadronic interaction code are shown in the last six plots of this paper. The spectrum, azimuthal and zenith angle distributions are shown in Figs. 9,10,11 for the SK site, and Figs. 12,13,14 for the SNO site. In these figures, the points and error bars are our data, the

higher sets of lines are from the BGS 1-D calculation[3], and the lower sets are from the 3-D calculation of Battistoni[8]. The results for each site arise from back-tracking 22×10^6 protons and 2.5×10^6 alphas. The number of neutrinos crossing each detector is 3.1×10^6 .

3.1 Fluxes

In overall fluxes, our results are in good agreement with Battistoni *et al.*, who use the same primary flux and a similar hadronic generator. The BGS[3] results are somewhat higher, largely due to differences in hadronic generators as noted above.

3.2 East-West Effect

The azimuthal angle distributions for the SK site are shown in Fig.10 and those for SNO are in Fig.13. After making the cuts proposed by Lipari[11], numerical values are given in table 1. Our model reproduces the correct hierarchy of East-West asymmetries, in order of highest to lowest: $\nu_e, \bar{\nu}_\mu, \nu_\mu, \bar{\nu}_e$. The lepton asymmetries are calculated by weighting the neutrino values with the quasi-elastic scattering cross sections[12] and convoluting with the neutrino lepton scattering angle. The mean value of this angle at these energies is 36° [10]. The much smaller effect of detector resolution is not taken into account; the same is true for Lipari's work. However, our lepton asymmetries are significantly higher than those of Lipari and SK data; the overall electron asymmetry is ~ 0.32 , and the muon asymmetry is ~ 0.23 . We note that a recent 3-D calculation of Wentz *et al.* [13] also reports large asymmetries. This needs further investigation.

3.3 Horizontal Enhancement

The zenith angle distributions for the SK site are shown in Fig.9 and those for SNO are in fig.12. The energy range is $0.5 \text{ GeV} < E_\nu < 3 \text{ GeV}$. Our calculations are presented with those of Bartol (1D) and Battistoni (3D). Lipari's horizontal enhancement can be seen in the 3D models, especially at the SNO site where neutrino spectrum is much softer. Honda *et al.* find a 10% smaller enhancement which they ascribe to their use of a different hadronic interaction model. This feature is not present in the 1D calculation. However, it is almost completely washed out in the detection of neutrino-induced leptons, as demonstrated in Refs. [8,14].

4 Conclusions

This work describes a full three-dimensional simulation of atmospheric neutrino fluxes. It largely justifies previous and widely used (1-D) approximations.

We note that the overall fluxes depend on our choice of hadronic code. We can discount GHEISHA which is known not to work too well at the low energies important in generating quasi-elastic leptons. That leaves CALOR/FRITIOF and GEANT-FLUKA, which produce very similar spectra, angular distributions, and fluxes.

We confirm the geometrical horizontal enhancement. The east-west asymmetries predicted by our model are higher than those of Lipari[11] and SK data[10], but similar to those of Wentz[13].

Acknowledgements

The authors would like to thank E. Kearns and C. Walter for the use of the Boston University Physics Department's O2000 CPU farm. We also thank T. Gaisser and P. Lipari for useful discussions. The work was supported by the Natural Science and Engineering Research Council of Canada (NSERC). One of us (YT) is grateful for a Faculty of Science scholarship from the University of British Columbia, and a summer studentship from the TRIUMF laboratory.

References

- [1] T. K. Gaisser, "Cosmic Rays and Particle Physics", (Cambridge 1992), p.85ff.
- [2] Y. Fukuda *et al.* (Super-Kamiokande collaboration), Phys. Rev. Lett. **81** (1999) 1562.
- [3] G. Barr, T. K. Gaisser and T. Stanev, Phys. Rev. **D39**, 3532 (1989).
- [4] M. Honda, K. Kasahara, K. Hidaka and S. Midorikawa, Phys. Lett. **B248**, 193 (1990).
- [5] E. V. Bugaev and V. A. Naumov, Phys. Lett. **B232**, 391 (1989).
- [6] H. Lee and Y. S. Koh, Nuovo Cimento **B105**, 883 (1990).
- [7] T. K. Gaisser, M. Honda, K. Kasahara, H. Lee, S. Midorikawa, V. Naumov and T. Stanev, Phys. Rev. **D54**, 5578 (1996).
- [8] G. Battistoni, A. Ferrari, P. Lipari, T. Montaruli, P. R. Sala and T. Rancati, Astroparticle Physics **12** (2000) 315-333.
- [9] P. Lipari, Astroparticle Physics **14** (2000) 153-170.
- [10] Futagami *et al.* (Super-Kamiokande collaboration), Phys. Rev. Lett. **82** (1999) 5194.
- [11] P. Lipari, Astroparticle Physics **14** (2000) 171-188.
- [12] C. H. Llewellyn-Smith, Physics Reports **3C** (1972) 262.
- [13] J. Wentz, A. Bercuci, D. Heck, H. J. Mathes, J. Oehlschläger, H. Rebel and B. Vulpesu, Proceedings of ICRC2001, 1167-1170.
- [14] M. Honda, T. Kajita, K. Kasahara and S. Midorikawa, Phys. Rev. **D64**, 053011 (2001).
- [15] J. Boger *et al.* (SNO collaboration), Nucl. Instr. Meth. **A449** (2000) 172-207.
- [16] L. V. Volkova, Sov. J. Nucl. Phys. **31** (1980) 784-790.
- [17] G. Barr, T. K. Gaisser and T. Stanev, Phys. Rev. **D38**, 85-94 (1988).
- [18] P. Lipari, T. Stanev and T. K. Gaisser, Phys. Rev. **D58** (1998) 073003
- [19] V. Agrawal, T. K. Gaisser, P. Lipari and T. Stanev, Phys. Rev. D **53**, (1996) 1314.
- [20] T. K. Gaisser, astro-ph/0104327, Astroparticle Physics...
- [21] Geomagnetic Field Models and Synthesis Software, Version 2.1 (1995), Geomagnetic Data Group, National Geophysical Data Center, World Data Center-A for Solid Earth Geophysics, 325 Broadway, E/GC1, Boulder, CO 80303. WWW address: <http://www.ngdc.noaa.gov/seg/potfld/geomag.html>

- [22] NASA, NOAA and US Air Force, US standard atmosphere 1976, NASA technical report NASA-TM-X-74335, NOAA technical report NOAA-S/T-76-1562 (1976)
- [23] CORSIKA code courtesy of Dieter Heck, Institut für Kernphysik 3, Forschungszentrum Karlsruhe, Postfach 3640, D-76021 Karlsruhe, Germany (<http://www-ik3.fzk.de/~heck/>).
- [24] GEANT Manual, Application Software Group, CERN program library long write-up W5013, CERN (Geneva) 1994. We use GEANT version 3.21 and the CALOR/GEANT interface 1.04/10 (1997).
- [25] A. Fassò, A. Ferrari, J. Ranft and P. R. Sala, Proc. IV Int. Conf. on Calorimetry in High Energy Physics, La Biodola (Elba), Ed. A. Menzione and A. Scribano, World Scientific p.493 (1993).
- [26] B. Nilsson-Almqvist and E. Stenlund, Computer Phys. Commun. **43** (1987) 387. The FRITIOF version used here is 7.02 by Hong Pi, 1993. The JETSET version is 7.3 (1991).
- [27] M. Messier, Ph.D thesis, Boston University 1999, p.120, unpublished (<http://www-sk.icrr.u-tokyo.ac.jp/doc/sk/pub/>).

Species	SK (data)	SK (Lipari)	SK (This Work)	SNO (Lipari)	SNO (This Work)
ν_e		0.335	0.390 ± 0.006	0.214	0.161 ± 0.015
$\bar{\nu}_e$		-0.065	0.158 ± 0.010	-0.061	-0.034 ± 0.027
ν_μ		0.028	0.223 ± 0.006	0.002	0.033 ± 0.010
$\bar{\nu}_\mu$		0.240	0.320 ± 0.005	0.153	0.094 ± 0.009
e	0.21 ± 0.04	0.224	0.32	0.136	0.11
μ	0.08 ± 0.04	0.091	0.23	0.046	0.05

Table 1

East-west asymmetries for each neutrino and lepton species, for the SK and SNO sites. Neutrinos are selected with $E = [0.5, 3.0]$ GeV (leptons with $[0.4, 3.0]$ GeV) and $\cos\theta < 0.5$. The SK data are from Ref. [10]. Lipari's values are from Ref. [11].

Figure Captions

Figure 1: Rigidity cutoffs in the 1-D model for SNO (top) and SK (bottom) sites. The more northerly SNO site has in general much lower cutoffs. The SNO site has the opposite up-down asymmetry to the SK site, and a very much smaller east-west asymmetry. These cutoffs were not used in the calculation, they are merely means to check part of the code, and as an aid to understanding. In terms of cardinal points the x-axis is ordered N-W-S-E-N.

Figure 2: The cutoff maps of Fig.1 can be understood in terms of the angle of the geomagnetic field as seen from the detector position. Because the dip angle at the SK site is small, there is a strong deficit of primaries coming from the east (see Fig.2. At the SNO site, the dip angle is large, so the east-west asymmetry is small, and there is almost no reduction in primaries coming from above. However, where the line-of-sight intersects the geomagnetic field at 90° , there is an increase in the cutoff. This occurs for near-horizontal primaries, and for those coming from a tilted ring around middle latitudes in the southern hemisphere.

Figure 3: Maps of the intensities of cosmic ray primaries on the earth's surface (averaged over all incident angles and shown as a fraction of the zero geomagnetic field case) are shown for 2,4,6,10,20 and 50 GeV/c. The two small white crosses mark the positions of SNO and SK.

Figure 4: Sketch of the proton + air nucleus $\rightarrow \pi \rightarrow \mu$ production and decay chain which leads to muons being observed deep underground in SNO. Pions decay in flight in the atmosphere to produce observable muons and neutrinos.

Figure 5: Spectrum-weighted moments for the production of charged pions as a function of proton total lab energy, for different common hadronic codes. The moment values are calculated by GHEISHA (low; $\circ \cdot \cdot \circ \cdot \cdot \circ$), CALOR (X - - - X - - - X), FRITIOF ($\cdot \text{---} \cdot \text{---} \cdot$) and GEANT-FLUKA (high; $\Delta \text{---} \Delta \text{---} \Delta$). For each calculation the higher of the two data sets represents π^+ production, and the lower, π^- . The main results of this work are obtained using GEANT-FLUKA. The combination with a spectrum-weighted moment which closely resembles that in BGS[7] is CALOR below 10 GeV/c and FRITIOF above 10 GeV/c.

Figure 6: Spectrum-weighted production of charged pions of 3-4 GeV/c as a function of primary energy. This momentum bin is responsible for neutrino production with energies around 1 GeV. This work (CALOR/FRITIOF: $\circ \text{---} \circ$) is compared with BGS ($\cdot \cdot \cdot \cdot \cdot$) [7].

Figure 7: This diagram shows how the relative bending of charged primaries

and secondaries contributes to the east-west asymmetry of the various neutrino species. The hierarchy of asymmetries is expected to be (high to low): $\nu_e, \bar{\nu}_\mu, \nu_\mu, \bar{\nu}_e$.

Figure 8: High and low energy atmospheric neutrinos are expected to have different zenith angle distributions. Both peak at the horizontal, but for different reasons. High energy neutrinos come from high energy mesons, which are produced collinearly with the almost isotropic primaries. However, they are more likely to decay in the greater path length of atmosphere at the horizontal. In contrast, low energy cascades lose all angular correlation with the primary, resulting in a purely geometrical enhancement at the horizontal.

Figure 9: Neutrino energy spectra for SK site. The data points are this work, using the GEANT-FLUKA hadronic code. The lines are calculations of other groups. Those with the horizontal peak are from the 3D model of Battistoni et al. [8]; the solid lines are neutrinos and the dotted antineutrinos. The lines with the slight horizontal dip are from the Bartol 1D model [19]; the dashed lines are neutrinos and the dash-dotted antineutrinos.

Figure 10: Neutrino azimuthal angle distributions for the SK site.

Figure 11: Neutrino zenith angle distributions for the SK site.

Figure 12: Neutrino energy spectra for the SNO site. The line conventions are the same as for SK.

Figure 13: Neutrino azimuthal angle distribution for the SNO site. Line convention as for SK. The horizontal enhancement is greater at SNO than at SK because the higher geomagnetic latitude softens the neutrino spectrum.

Figure 14: Neutrino zenith angle distribution for the SNO site. Line convention as for SK. The horizontal enhancement is greater at SNO than at SK because the higher geomagnetic latitude softens the neutrino spectrum.

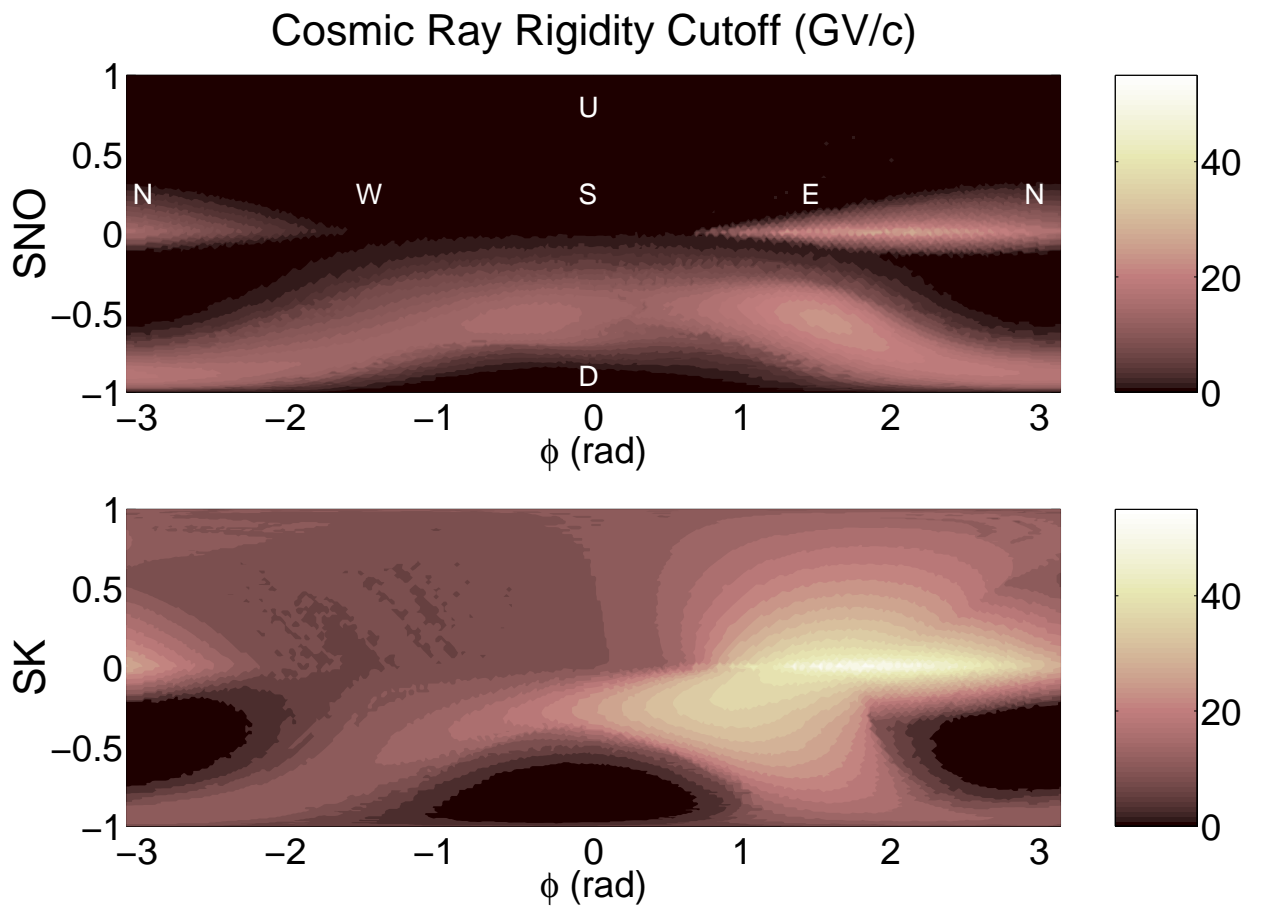


Fig. 1.

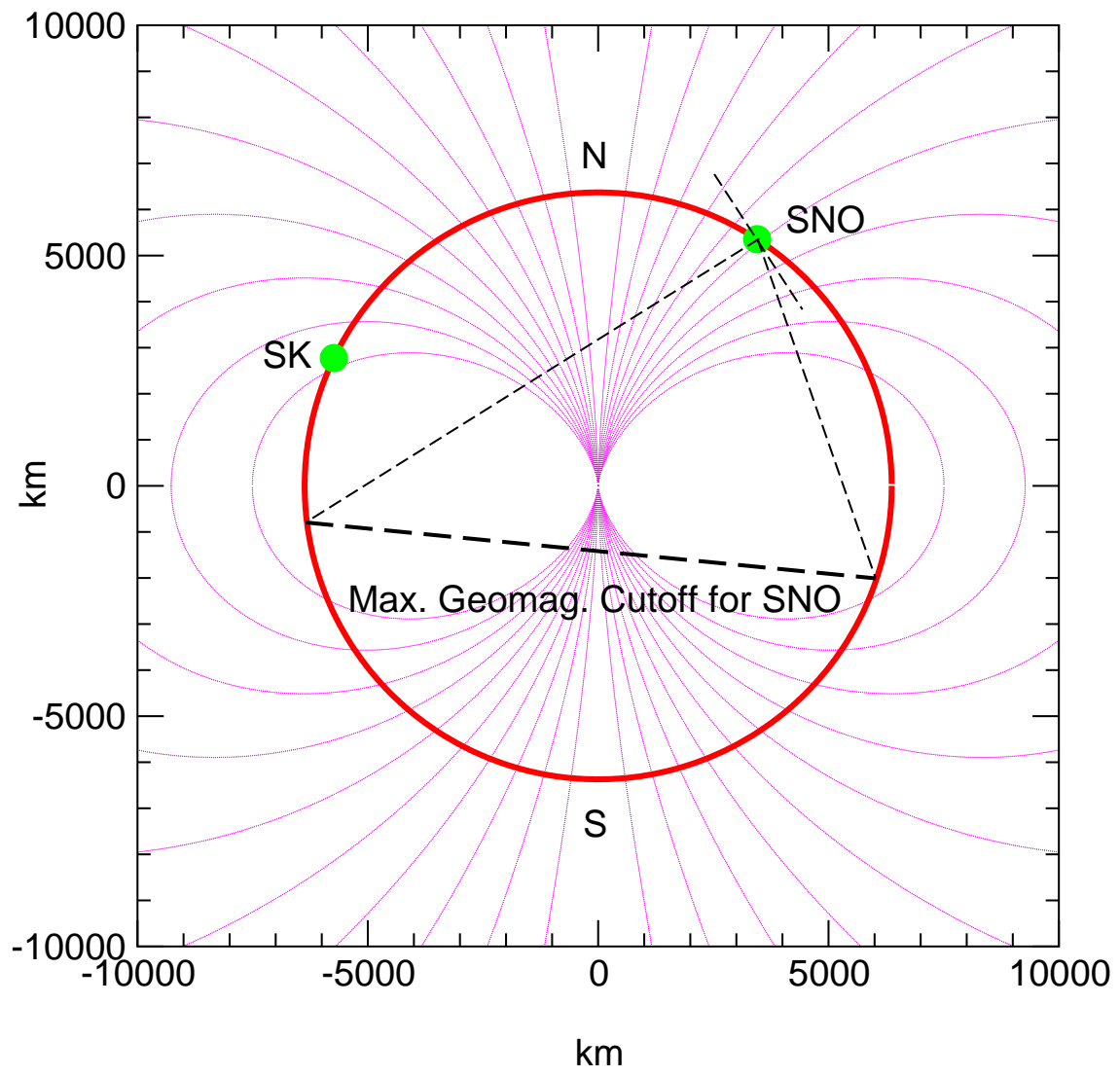


Fig. 2.

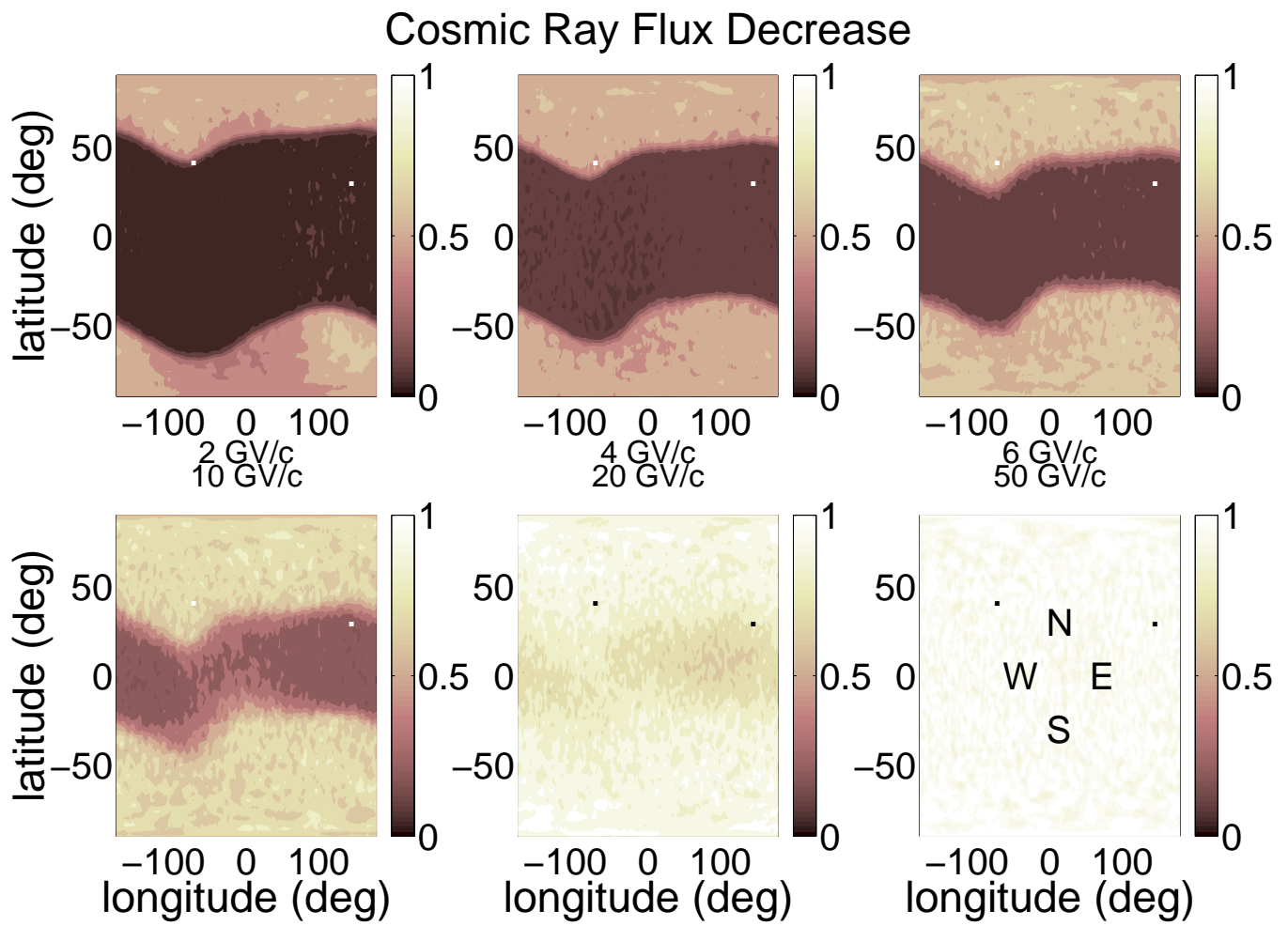
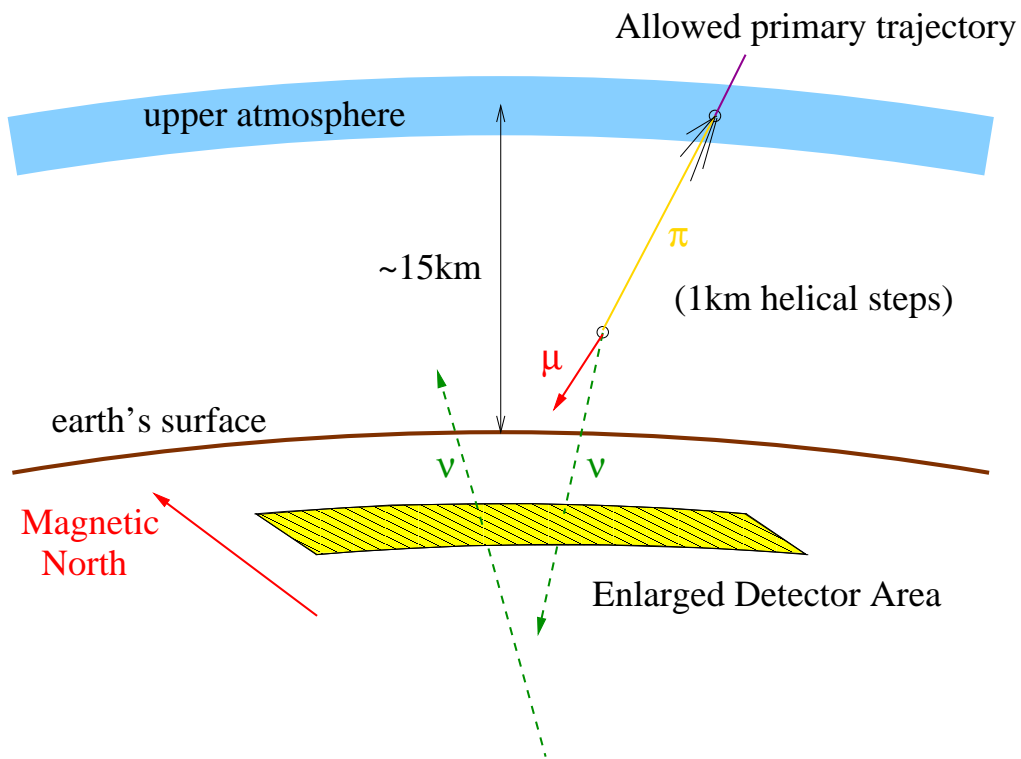


Fig. 3.

3-D Tracking of Cosmic Ray Secondaries



waltham/sno/an/yaro/astropp/3d_an.fig 00/06/27

Fig. 4.

Charged π Spectrum Weighted Moments

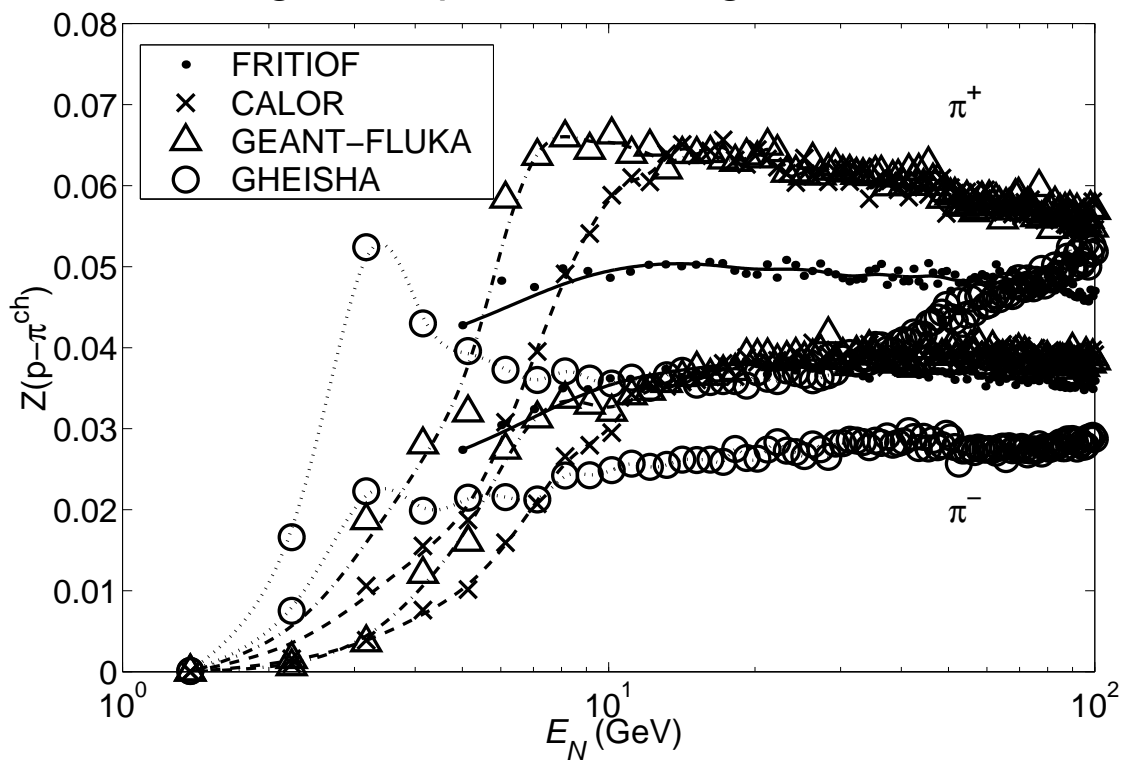


Fig. 5.

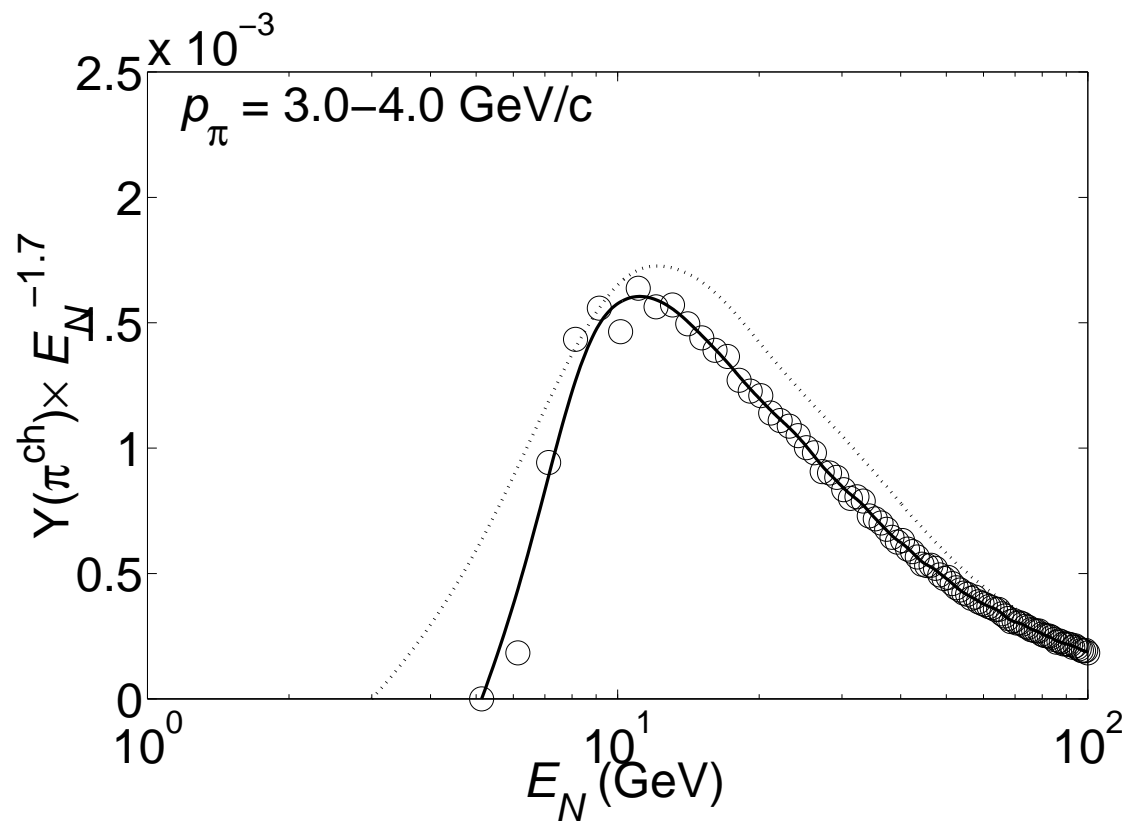


Fig. 6.

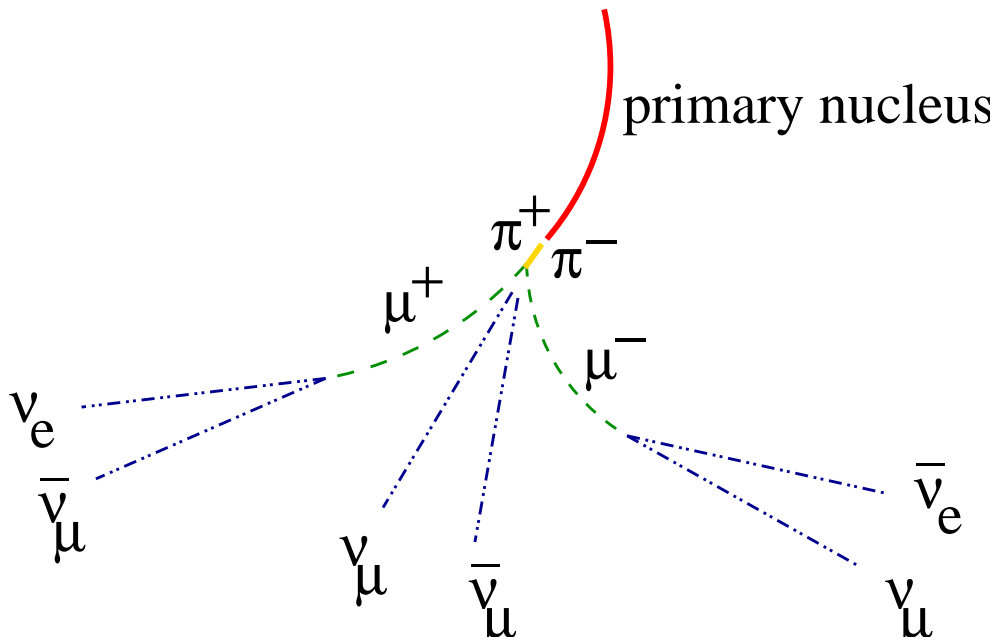


Fig. 7.

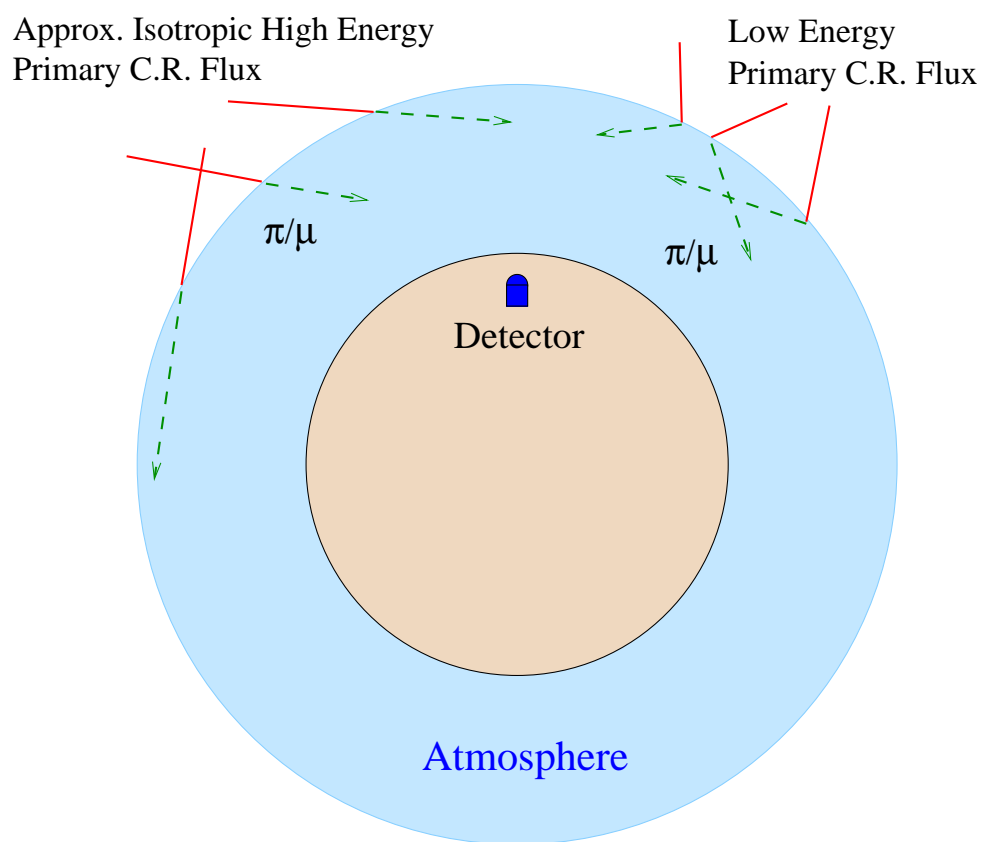


Fig. 8.

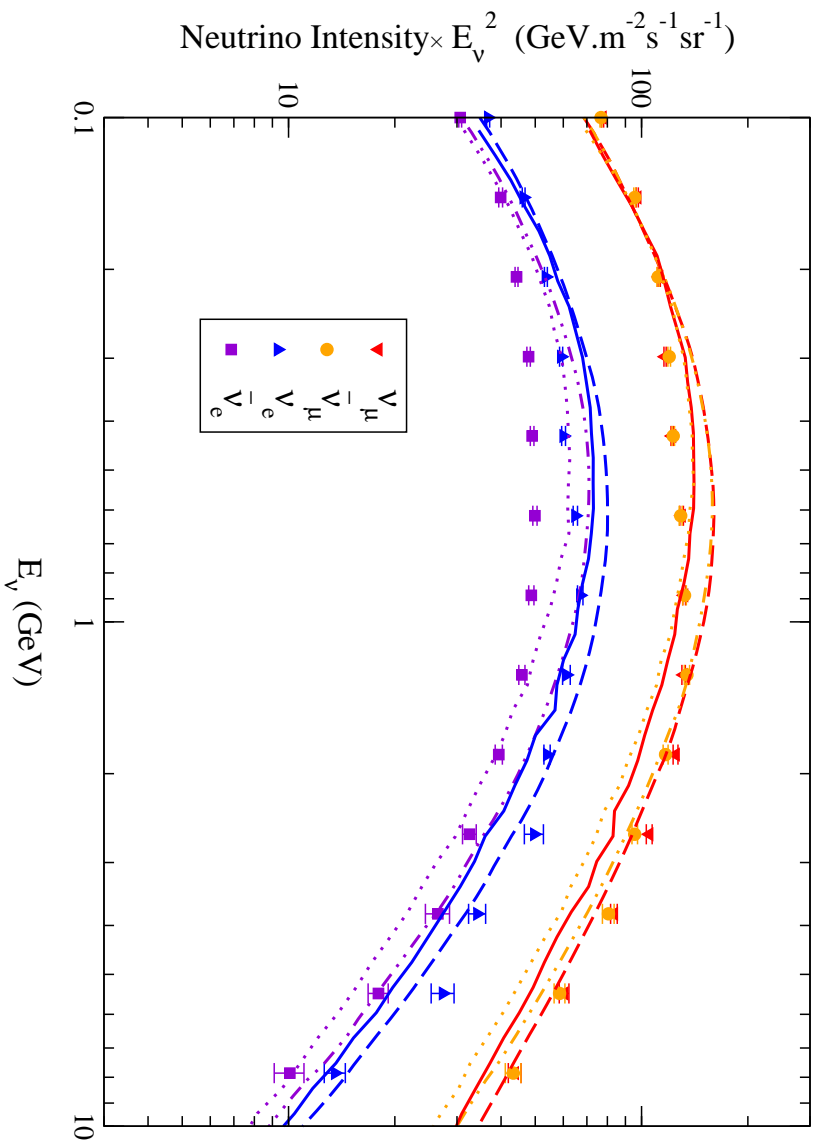


Fig. 9.

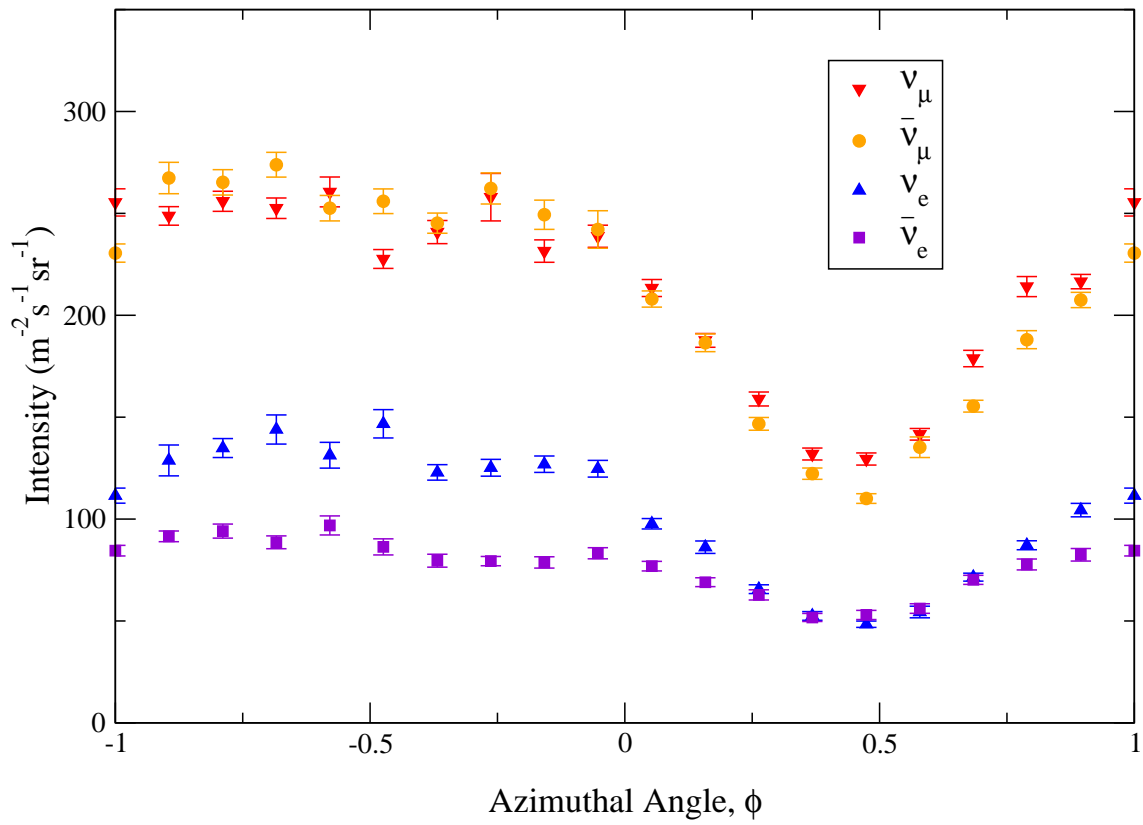


Fig. 10.

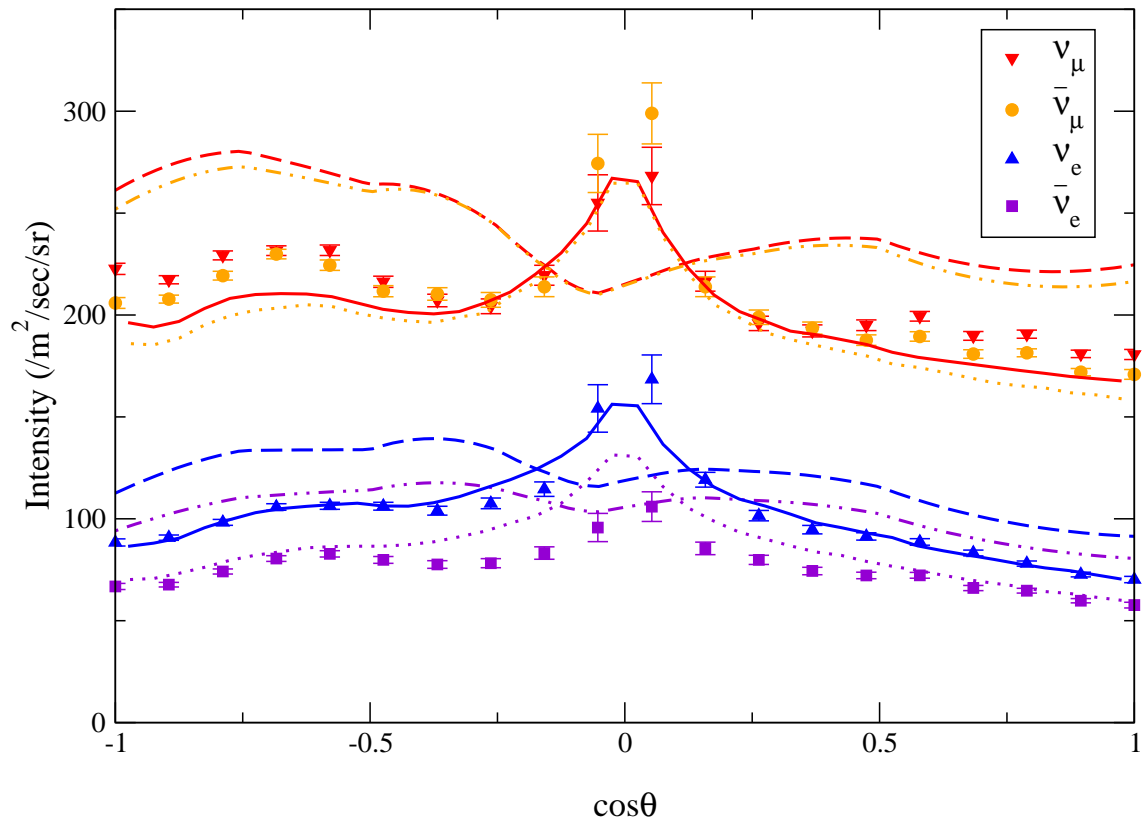


Fig. 11.

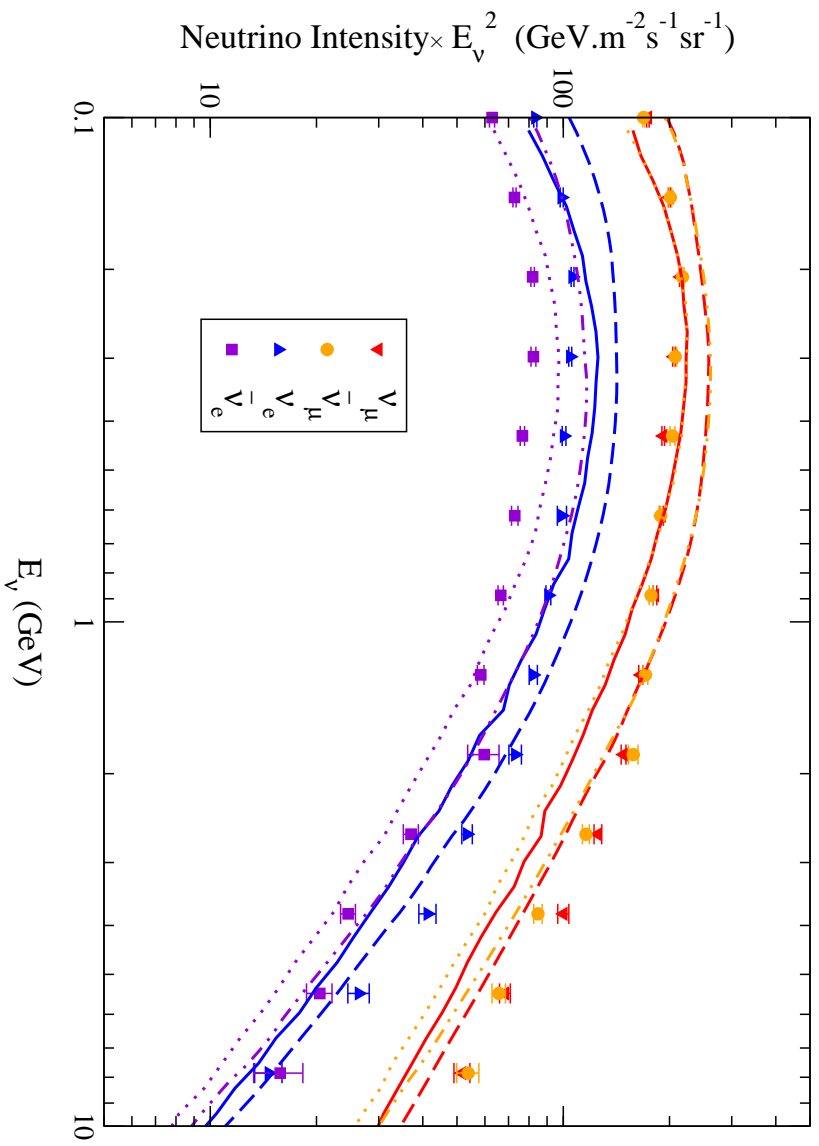


Fig. 12.

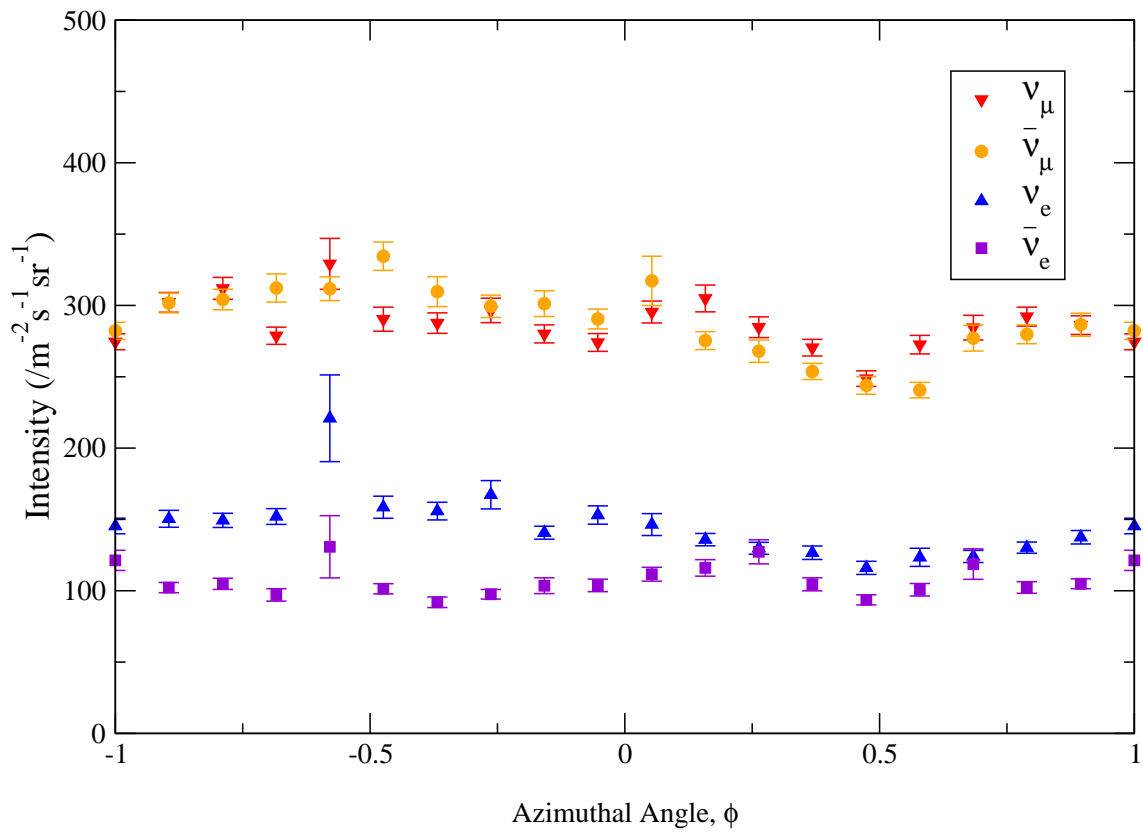


Fig. 13.

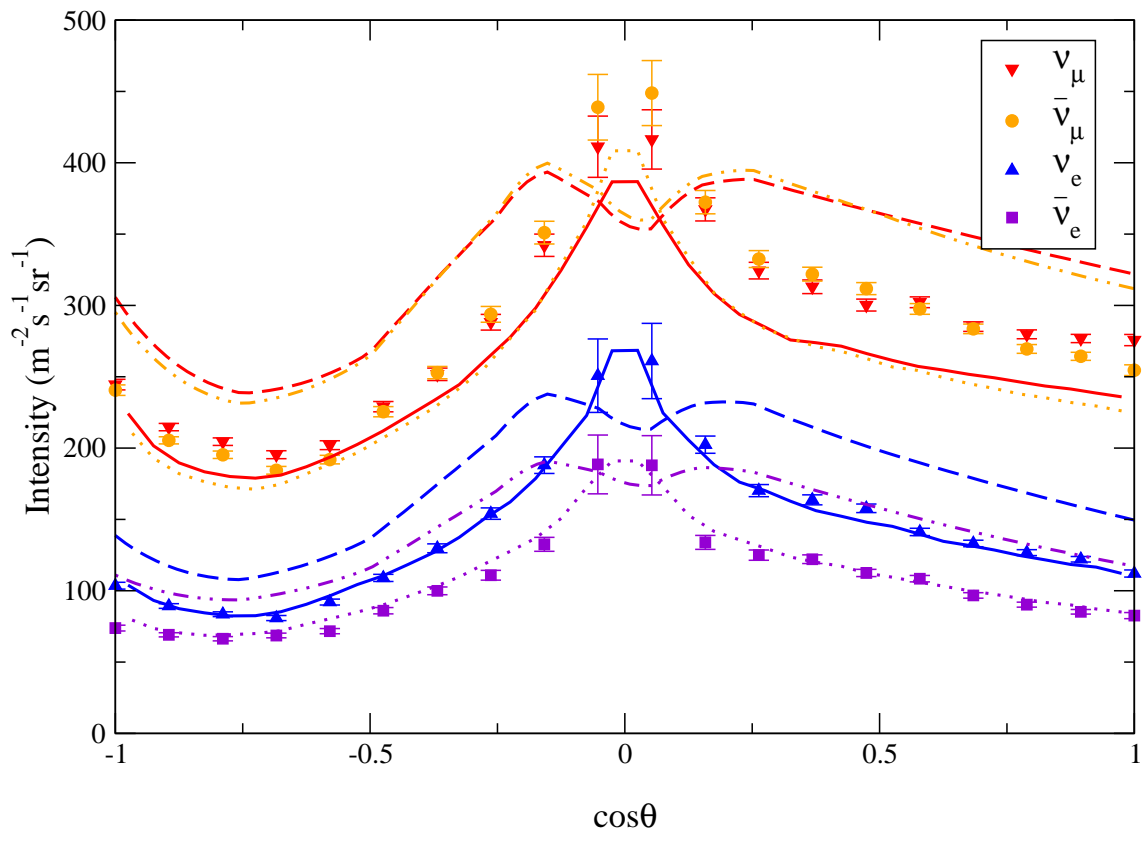


Fig. 14.